An instability theory for the formation of ribbed moraine, drumlins and mega-scale glacial lineations

A. C. Fowler[1,2] and M. Chapwanya[3]

[1]MACSI, University of Limerick, Limerick, Ireland
[2]OCIAM, University of Oxford, Oxford, UK
[3]Department of Mathematics and Applied Mathematics, University of Pretoria, South Africa

August 5, 2014

Abstract

We present a theory for the coupled flow of ice, subglacial water, and subglacial sediment, which is designed to represent the processes which occur at the bed of an ice sheet. The ice is assumed to flow as a Newtonian viscous fluid, the water can flow between the till and the ice as a thin film, which may thicken to form streams or cavities, and the till is assumed to be transported, either through shearing by the ice, squeezing by pressure gradients in the till, or by fluvial sediment transport processes in streams or cavities.

In previous studies, it was shown that the dependence of ice sliding velocity on effective pressure provided a mechanism for the generation of bedforms resembling ribbed moraine, while the dependence of fluvial sediment transport on water film depth provides a mechanism for the generation of bedforms resembling mega-scale glacial lineations (MSGL). Here we combine these two processes in a single model, and show that, depending largely on the granulometry of the till, instability can occur in a range of types which range from ribbed moraine through three-dimensional drumlins to mega-scale glacial lineations.

Keywords: Drumlins, ribbed moraine, mega-scale glacial lineations, instability.

1   Introduction

Drumlins are small, rounded hills which occur in swarms. On the ground they give rise to a typically rolling landscape, which can, for example, be found in large parts of Ireland (where they were first distinctively observed). Where they become inundated, they are particularly remarkable, as the individual hills then stand out, as shown in

Figure 1: A view from Westport harbour, Co. Mayo, Ireland, of some of the drumlins of Clew Bay.

figure 1, which is a view from Westport harbour in Co. Mayo of the drumlins of Clew Bay.

The aspect of pattern which is evident on the ground in many drumlin fields is particularly noticeable in satellite photographs, or even better in digital elevation models such as that in figure 2, which shows that the drumlins of north central Ireland blanket the entire landscape.

The origin of these landforms has been a subject of discussion for well over a hundred years. Early investigators such as Bryce (1833) correctly perceived of drumlins as being formed by the transport of sediments. Bryce was able to determine, by examination of the kinds of rocks in the till which formed drumlins in Northern Ireland, that they had formed through the action of a current which had swept down from the northwest. Those being diluvial times, Bryce assumed this was a current of water. It was not until Agassiz's glacial theory that opinion changed, and Kinahan and Close (1872), describing the drumlins in the vicinity of Clew Bay, associated them squarely with the flow of the great ice sheets of the ice age. Over the following century, the debate on origin largely centred on the alternative concepts of erosional or depositional origin (e. g., Gravenor 1953), but this period is remarkable by its absence of any quantitative theory. It was with the work by Smalley and Unwin (1968), Menzies (1979a) and Boulton (1987), that the rôle of deforming till was explicitly considered; but still there was no descriptive theory. Only with the landmark paper of Hindmarsh (1998) was the interaction between ice flow and deformable sediment
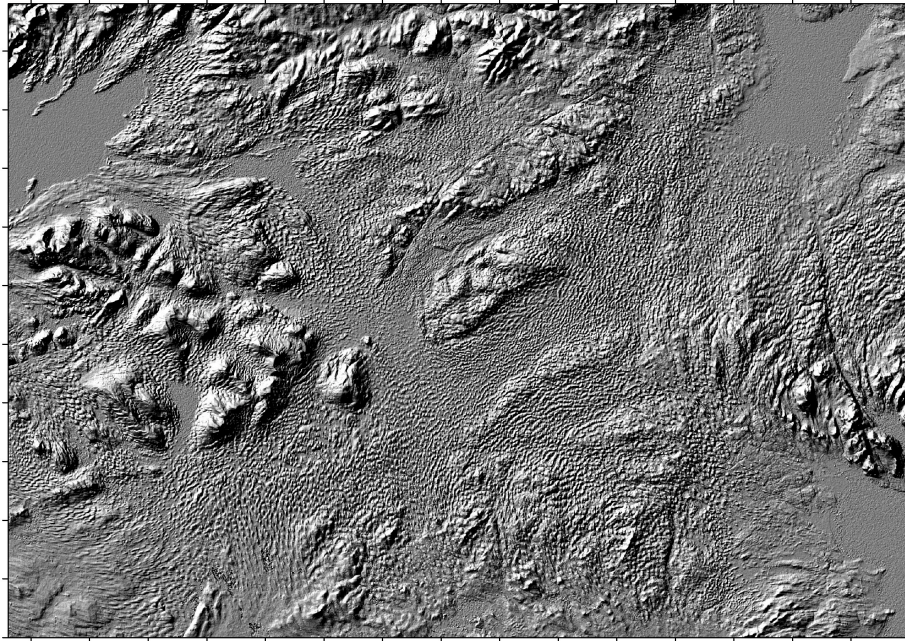
Figure 2: A digital elevation model of the drumlins of north central Ireland. The drumlins are the small scale asperities which cover the landscape. Donegal Bay is visible at top left, and Lough Neagh at top right. Width of field is about 150 km.

formulated mathematically, with the result that instability could be predicted to occur with wavelengths of several hundred metres, corresponding to those which are observed.

Hindmarsh's numerical study was followed by an analytic study by Fowler (2000), which yielded similar conclusions. This promising beginning has since run into theoretical obstacles, as described in the studies by Schoof (2007a,b). There are three issues which arise. The first is a practical one: as the bedforms grow, they soon reach an amplitude where the ice separates from the till bed, forming lee-side cavities. Cavitation is not in itself a problem, but it raises severe difficulties in continuing the numerical evolution of the bedforms. Schoof circumvented this by seeking travelling wave solutions, and suggested that the resulting bedforms would be of insignificant elevation compared to the tens of metres which can be obtained.

A second difficulty is that the instability described by Hindmarsh (1998) and Fowler (2000) is fundamentally two-dimensional in nature. The difficulty here is that drumlins are three-dimensional objects, although it is not at all necessary that the initial instability be three-dimensional. Despite this, the search for three-dimensional waveforms has been elusive. Schoof (2007a) thought that the two-dimensional nature of the instability represented a serious obstacle to the theory, a view taken on trust by Pelletier (2008). Consideration of this issue represents one of the purposes of the present paper.

A third consideration concerns the stratigraphy of drumlins. While many consist

of an essentially homogeneous mass of till, there are certain fields of drumlins which provide evidence of stratification, and at first sight this seems incompatible with a formation mechanism which involves deformation of the till; the point has been emphasised by Hart (2005, p. 194) and Hiemstra *et al.* (2011), for example. A little thought shows that this is not a real objection in net-erosive environments, and indeed most of the principal stratigraphic constituents of drumlins can be plausibly explained (Stokes *et al.* 2013a).

The first difficulty alluded to above, and in effect also the third, was addressed by Fowler (2009), who devised a method to compute the evolution of drumlins after cavitation occurred. He incidentally found that the resulting waveforms became stationary, thus allowing the erosional mechanism of Stokes *et al.* (2013a) to provide an explanation for layered stratigraphy. The present paper addresses the second issue discussed above, that of the formation of three-dimensional bedforms.

It is a long-standing concept in theories of subglacial bedform genesis (e. g., Sugden and John 1976) that drumlins form part of a continuum traversed as some critical parameter varies, between the extremes of ribbed moraine (Dunlop and Clark 2006) and MSGL (Clark 1993). This attractive idea is predicated on the notion that one single mechanism can encompass the whole variety of bedforms, but it is by no means obvious that this is the case. Indeed, apart from the Hindmarsh–Fowler instability theory, a number of alternative explanations have been put forward to explain ribbed moraine, drumlins and MSGL (e. g., Fisher and Shaw (1992), Kleman and Hättestrand (1999), Hättestrand and Kleman (1999), Lindén *et al.* (2008), Lundqvist (1969), Möller (2006), Möller (2010) and Schoof and Clarke (2008)). An early review of drumlin formation theories is that of Menzies (1979b), and a more recent one is that of Clark (2010).

Schoof's (2007a) comments drove Dunlop *et al.* (2008) to the defensive position of advocating the instability theory only in connection with ribbed moraine formation, with the implicit recognition that ribbed moraine and drumlins were somehow different, and this informal distinction has gained a certain currency. It is not, however, one that we espouse, and indeed the principal purpose of the present paper is to show that a suitable model describing combined ice, sediment and water flow can indeed plausibly explain the whole spectrum of bedforms, from ribbed moraine through drumlins to MSGL. Before we commence this however, we need to describe and distinguish the various components of the instability theory as it has been developed thus far.

Hindmarsh (1998), Fowler (2000) and Schoof (2007a) all developed a theory based on the Stokes flow of ice near the bed (i. e., the ice surface is far away, so that the ice thickness is effectively infinite), with the ice assumed to be Newtonian viscous, and an underlying motion of water-saturated deformable till, described by an Exner equation for the ice/till interface, in which the till flux q is assumed to depend on basal shear stress τ and effective pressure N. The effective pressure is defined by

$$N = p_i - p_w, \qquad (1.1)$$

where p_i is ice pressure, which can be assumed known, and p_w is the basal water pressure at the ice/till interface, which must be determined. Hindmarsh, Fowler and

Schoof all assume this water pressure is in hydrostatic equilibrium, presumably with a subglacial drainage system at a (locally) constant effective pressure.

Fowler (2010a) extends the theory to ice of finite depth, and also treats three-dimensional perturbations, something also done by Schoof (2007a). An evolution of the theory is offered by Fowler (2010b), who finally considers the water flow as an active contributor to the model. That edition of the theory concerns MSGL, which are found via an instability analogous to the Smith–Bretherton theory of sub-aerial rivulet formation (Smith and Bretherton 1972). Fowler describes water flow either as a groundwater flow through porous till, or as a separated Poiseuille-like flow. When the water layer is absent, till deforms as before, but when the water layer is present, sediment transport occurs as interfacial bedload, and it is this latter which drives the rill-like instability.

In order to formulate a meaningful instability problem, Fowler adopted the stance of Creyts and Schoof (2009) that a possible subglacial drainage mechanism is that of a thin film trickling at the base of a glacier. The concept circumvents the Walder (1982) instability problem by allowing clast sizes larger than the film thickness. In retrospect, this seems the obvious basic flow, which takes account of the roughness of the bed. In the present paper, we adopt this viewpoint from the outset, thus allowing a sediment layer and a water layer to exist everywhere under the ice. The Fowler (2010b) MSGL model is thus modified by replacing through-till porous flow by a distributed film flow. The hydraulic potential in this water layer is to be determined, and in particular the stream system becomes part of the problem to be solved; and in fact, there is no theoretical distinction to be made between stream and cavity; they are both simply regions of separated flow.

The structure of the remainder of the paper is as follows. In section 2 we re-expound the Hindmarsh instability theory in its present form. Our presentation is a compact summary of the successive constituent sub-models of ice flow, water flow, sediment transport and ice closure, the last of these being a new development consequent on our assumption of a Creyts–Schoof water film. These sub-models are wiritten dimensionlessly, dimensionless parameters are estimated, and an asymptotically simplified model is then presented, combining the four sub-models.

Section 3 provides a uniform steady solution, and its linear stability is analysed; it is shown that the growth rate is determined by the solution of a quadratic equation, whose roots are plotted in terms of horizontal and transverse wavenumbers as functions of a critical parameter Π. Section 4 forms the conclusions of the study, in which also the meaning and interpretation of the results are discussed.

2   The instability theory

The Hindmarsh instability theory is built around a description of ice, water and sediment flow on a local horizontal scale of kilometres. The geometry of the flow is shown in figure 3. The coordinates are x, y, z, with z vertical, and x in the downstream ice flow direction. The ice surface is at $z = z_i$, the ice base and water surface at $z = s$, and the water base and sediment surface is at $z = b$. The water
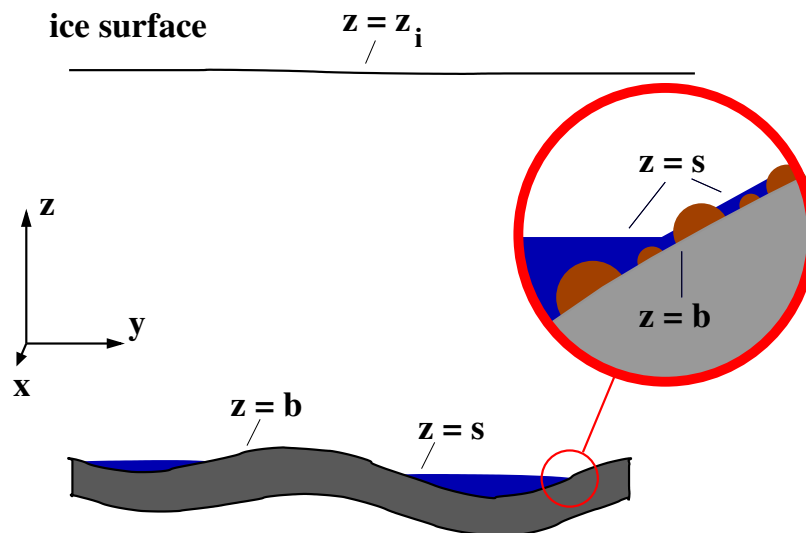
Figure 3: Schematic representation of model geometry (colour online). Ice with surface $z = z_i$ lies above sediment and water. The sediment surface is denoted by $z = b$, and the water surface (also the base of the ice) is denoted $z = s$. The x axis points down the ice upper surface, in the direction of flow. The view is from downstream, and represents a configuration consisting of subglacial streams in the troughs between glacial lineations. The inset shows the detail of the small scale roughness in the Creyts–Schoof water film.

depth is thus

$$h = s - b. \tag{2.1}$$

In the following subsections, we briefly describe the model equations for ice, water and sediment flow. Much of this can be found in the papers by Fowler (2010a,b), to which further reference should be made. For a more general introduction to models of ice flow, sediment transport and rivulet dynamics, see Fowler (2011), chapters 5,6 and 10.

2.1 Ice flow

The Stokes flow equations for the flow of ice, treated as a Newtonian viscous fluid, are given by (2.5) of Fowler (2010a), and are

$$
\begin{aligned}
\boldsymbol{\nabla}.\mathbf{u} &= 0, \\
\mathbf{0} &= -\boldsymbol{\nabla}P - \rho_i g \boldsymbol{\nabla} z_i + \eta_i \nabla^2 \mathbf{u},
\end{aligned}
\tag{2.2}
$$

where P is reduced pressure (ice pressure minus cryostatic pressure), $\mathbf{u}$ is ice velocity, ρ_i is ice density, g is the acceleration due to gravity, and η_i is the assumed constant ice viscosity. Defining the horizontal shear stress vector as

$$\boldsymbol{\tau} = (\tau_1, \tau_2), \tag{2.3}$$

($\tau_1 = \tau_{13}$ and $\tau_2 = \tau_{23}$ are the two horizontal components of shear stress), the surface boundary conditions are the stress balance and kinematic conditions

$$P - \tau_{nn} = 0, \quad \boldsymbol{\tau} = \mathbf{0},$$

$$w = z_{i,t} + u z_{i,x} + v z_{i,y} - a \quad \text{at} \quad z = z_i, \tag{2.4}$$

where subscripts t, x, y denote partial derivatives, a is the accumulation rate, and $\mathbf{u} = (u, v, w)$. The basal boundary conditions are then the sliding law and the kinematic boundary condition (ignoring the relatively small melting term), thus

$$\boldsymbol{\tau} = \frac{f(u_b, N)\mathbf{u}_b}{u_b},$$

$$w = s_t + u s_x + v s_y, \quad \text{at} \quad z = s, \tag{2.5}$$

where $\mathbf{u}_b = (u, v)$, evaluated at $z = s$, and called the sliding velocity; N is the effective pressure introduced in (1.1). To be specific, we will assume a generalised Weertman sliding law of the form

$$f(u_b, N) = R N^b u_b^c, \tag{2.6}$$

where R is a roughness coefficient (Bindschadler 1983).

The Stokes equations require two boundary conditions at top and bottom, so that the kinematic condition in (2.4) determines z_i, and we see from (2.5) that if s, s_t and N are known then the ice flow is fully determined. Before proceeding to water and sediment flow, we complete an approximate solution for the ice flow, based on the assumption of small basal ice slope, $|\boldsymbol{\nabla} s| \ll 1$, which is an accurate assumption.

Non-dimensionalisation

Following Fowler (2010a), we define the bedform elevation scale d_D, the till deformation scale d_T and the bedform length scale l_D, by

$$d_D = \frac{\tau_b}{\Delta \rho_{wi} g}, \quad d_T = \frac{\tau_b}{\Delta \rho_{sw} g (1 - \phi)}, \quad l_D = \left(\frac{\eta_i u_0 d_D}{\tau_b} \right)^{1/2} = \left(\frac{\eta_i u_0}{\Delta \rho_{wi} g} \right)^{1/2}, \tag{2.7}$$

where u_0 and τ_b are velocity and stress scales (defined below), ϕ is sediment porosity, and

$$\Delta \rho_{wi} = \rho_w - \rho_i, \quad \Delta \rho_{sw} = \rho_s - \rho_w, \tag{2.8}$$

with ρ_s being the sediment particle density and ρ_w the water density. This is equivalent to Fowler (2010a) if his effective pressure scale $N_c = \tau_b$.

The aim of the instability theory is to study perturbations about a uniform state, which we take to be the shear profile

$$\mathbf{u} = \left[u_0 + \frac{\tau_b}{\eta_i} \left(z - \frac{z^2}{2d_i} \right) \right] \mathbf{i}, \tag{2.9}$$

where

$$\tau_b = \rho_i g d_i S, \quad S = -\frac{\partial z_i}{\partial x}. \tag{2.10}$$

7

Here d_i is the ice depth; obviously this varies over the scale of the ice sheet, but can be taken as a constant on the much smaller bedform length scale l_D. The values of u_0 and the downstream ice surface slope S (or τ_b) are determined from the ice sheet model at a much larger length scale, and can be taken to be given in the present context.

We now scale the ice flow equations by writing

$$s \sim d_D, \quad \mathbf{x} = l_D \mathbf{x}^*, \quad p_e, N, P, \tau_{nn}, \tau, f \sim \tau_b, \quad z_i = d_i[1 - \sigma S x^* + SH], \quad a \sim S u_0,$$

$$\mathbf{u} = \left[u_0 \bar{u} + \frac{\tau_b}{\eta_i} \left(z - \frac{z^2}{2d_i} \right) \right] \mathbf{i} + \nu u_0 \mathbf{u}^*, \quad u_b \sim u_0, \quad t \sim t_D = \frac{d_D l_D}{d_T u_0} \equiv \frac{\Delta \rho_{sw}(1 - \phi) l_D}{\Delta \rho_{wi} u_0},$$

$$\tag{2.11}$$

where the bed aspect ratio ν and corrugation parameter σ are defined by

$$\nu = \frac{d_D}{l_D}, \quad \sigma = \frac{l_D}{d_i}. \tag{2.12}$$

The asterisks on $\mathbf{u}^*$ and $\mathbf{x}^*$ are omitted in the sequel. The dimensionless mean basal velocity $\bar{u}$, which equals one in the basic shear flow, does not necessarily remain so, as the development of bedforms will alter it. Note that with the sliding law of the form (2.6), the dimensionless sliding law is

$$f(u_b, N) = R^* u_b^c N^b, \tag{2.13}$$

where R^* is defined by

$$R^* = \frac{R u_0^c}{\tau_b^{1-b}}. \tag{2.14}$$

For small ν, the bed conditions at $z = \nu s$ can be linearised to apply at $z = 0$, and because $S \ll 1$, the ice surface conditions can be linearised to apply at $z = 1$. The perturbed ice flow thus satisfies the biharmonic equation in the strip $0 < z < 1$ and can be solved by Fourier transform using the prescribed stress conditions at the ice surface, together with the sliding law and the normal stress at the bed. Specifically, if we define

$$\Phi = P - \tau_{nn} + H, \quad F = f(\bar{u}, N) - 1 \tag{2.15}$$

(Fowler (2010a) wrote $\Phi = -\Theta$), then the kinematic conditions at the bed and the ice surface take the dimensionless form

$$\alpha s_t + \bar{u} s_x = w, \quad \lambda H_t = \Xi \tag{2.16}$$

(Fowler wrote $w = K$), where

$$\alpha = \frac{d_T}{d_D} \equiv \frac{\Delta \rho_{wi}}{\Delta \rho_{sw}(1 - \phi)}, \quad \lambda = \frac{\alpha S}{\nu \sigma} \equiv \frac{(\Delta \rho_{wi})^2}{\rho_i \Delta \rho_{sw}(1 - \phi)}, \tag{2.17}$$

and w and Ξ can be written as linear combinations of H, F and Φ; additionally $\bar{u}$ is defined by the horizontal force balance

$$\overline{f(\bar{u}, N)} = 1; \tag{2.18}$$

8

the overline denotes a spatial average (so $\bar{u}$ is a function of time only). It follows from this and (2.13) that

$$f(\bar{u}, N) = N^b / \overline{N^b}. \tag{2.19}$$

In detail, defining the Fourier transform of a function

$$\hat{f}(\mathbf{k}) = \int_{-\infty}^{\infty} \int_{-\infty}^{\infty} f(x, y) e^{ik_1 x} e^{ik_2 y} \, dx \, dy, \tag{2.20}$$

where $\mathbf{k} = (k_1, k_2)$, and k_1 and k_2 are downstream and transverse wave numbers, respectively, we obtain

$$\begin{aligned}
\hat{\Phi} &= -\frac{2k}{\Delta_5} \left[2\hat{H} + 2G_{23}\hat{F} - (G_{21} + G_{22})\hat{w} \right], \\
\hat{\Xi} &= G_{27}\hat{H} + G_{28}\hat{F} + G_{29}\hat{w},
\end{aligned} \tag{2.21}$$

where the various coefficients are defined by Fowler (2010a)). Since $\lambda \sim 10^{-2}$ is small, we can put $\Xi = 0$, and simplification of (2.21) yields an expression for $\hat{w}$:

$$\hat{w} = \frac{S_h^2}{2k(j + S_h C_h)} \hat{\Phi} + \frac{ik_1 j}{2k^2(j + S_h C_h)} \hat{F}, \tag{2.22}$$

where

$$j = \frac{k}{\sigma}, \quad k = (k_1^2 + k_2^2)^{1/2}, \quad S_h = \sinh j, \quad C_h = \cosh j. \tag{2.23}$$

In summary, the calculation of ice flow over the bed yields a dimensionless evolution equation for s of the form

$$\alpha s_t + \bar{u} s_x = w = J * \Phi + L * F, \tag{2.24}$$

where the asterisk denotes the Fourier convolution, and the transforms of J and L are

$$\hat{J} = \frac{S_h^2}{2k(j + S_h C_h)}, \quad \hat{L} = \frac{ik_1 j}{2k^2(j + S_h C_h)}. \tag{2.25}$$

2.2 Water flow

In dimensional terms, the hydraulic potential can be shown to be

$$\psi = \rho_i g(z_i - d_i) + \Delta \rho_{wi} g s - N + P - \tau_{nn}. \tag{2.26}$$

The earliest versions of the instability theory assumed constant ψ; this is possible, but as we shall see, unlikely.

Slow water flow through a thin film or stream of depth h is given by a local Poiseuille flow, and takes the form

$$h_t = \boldsymbol{\nabla} \cdot \left[\frac{h^3}{12\eta_w} \boldsymbol{\nabla} \psi \right] + \Gamma, \tag{2.27}$$

where η_w is water viscosity and Γ is the local water source due to internal melting in the basal ice, and is given approximately by

$$\Gamma = \frac{G + \tau_b u_0 - q_T}{\rho_w L}; \tag{2.28}$$

here G is geothermal heat flux, q_T is heat flux into the ice, and L is latent heat. The dependence of Γ on ice flow may have a dynamical effect on a large scale (Kyrke-Smith *et al.* 2014), but in fact Γ is negligible on the small length scale of concern here.

We scale these equations using values in (2.11), and in addition

$$\psi \sim \tau_b, \quad h \sim h_0, \tag{2.29}$$

where h_0 is a typical size of the water film depth, prescribed below; this leads us to the dimensionless forms,

$$\begin{aligned}
\psi &= -\sigma x + s - N + \Phi, \\
\varepsilon \omega h_t &= \boldsymbol{\nabla} \cdot \left[h^3 \boldsymbol{\nabla} \psi \right] + \omega.
\end{aligned} \tag{2.30}$$

The definitions of the parameters are best framed in terms of the order of magnitude q_w of the basal water flux, given by

$$q_w = \Gamma l_i = \frac{h_0^3 \tau_b}{12 \eta_w l_i}, \tag{2.31}$$

where l_i is a relevant horizontal length scale for the large scale ice flow. (2.31) thus defines a mean film thickness

$$h_0 = \left(\frac{12 \eta_w l_i^2 \Gamma}{\tau_b} \right)^{1/3}, \tag{2.32}$$

as well as the parameters

$$\varepsilon = \frac{h_0}{\Gamma t_D}, \quad \omega = \frac{l_D^2}{l_i^2}; \tag{2.33}$$

t_D was defined in (2.11).

2.3 Sediment flow

Next, we write a suitable Exner equation (describing conservation of the mobile sediment) for the evolution of the sediment surface $z = b$. This amalgamates the till flux terms described in the original instability theory, e. g., Fowler (2010a), and the sediment transport terms appropriate for fluvial flow described by Fowler (2010b). We take it in the form

$$\begin{aligned}
b_t + \boldsymbol{\nabla} \cdot \left[\tfrac{1}{2} u_0 \bar{u} h_A \mathbf{i} - \frac{h_A^3}{12 \eta_s} \boldsymbol{\nabla} N \right] &= -E - \boldsymbol{\nabla} \cdot \left[\frac{Q(\tau_e)}{\tau_e} \boldsymbol{\tau}_e \right], \\
\boldsymbol{\tau}_e &= - \left\{ \tfrac{1}{2} h \boldsymbol{\nabla} \psi + \Delta \rho_{sw} g D_s \boldsymbol{\nabla} b \right\}.
\end{aligned} \tag{2.34}$$

The flux term on the left comprises an advective term representing a shearing by the overlying ice flow, and a diffusive term representing till squeezing in a relatively thin layer; h_A is the thickness of the deforming till, which is limited by the yield stress μN, thus (Fowler 2009)

$$h_A = \frac{\left[\left[\frac{\tau}{\mu} - N\right]\right]\Big|_+}{\Delta\rho_{sw}(1 - \phi)g},$$ (2.35)

where μ is the coefficient of friction; here $\tau = f(\bar{u}, N)$ is the basal shear stress. As often, the till flux assumes here an effective viscosity η_s, corresponding to a yield stress material with the normal flow rule, and as always, this does not imply the till is viscous, but the application of more likely rheologies (e. g., Henann and Kamrin 2013) is an uncertain distraction to the present purpose.

The terms on the right represent net suspended sediment erosion (E), which we take to be zero, indicating a balance between suspended sediment erosion and deposition. The term inside square brackets represents bedload sediment transport Q, and is generally non-zero and increasing downstream, as the glacier strips its bed away. The second equation defines the effective stress $\boldsymbol{\tau}_e$ transmitted by the water flow to the bed, consisting of the actual viscous stress in the water plus a term representing the propensity of sediment grains to roll downhill: D_s is the sediment grain size. b in this equation was written as s in equation (2.19) of Fowler (2010b), on the basis that h is small; (2.34) is the correct form, however; cf. Fowler *et al.* (2007), equation (2.3). The bedload Q will generally be a nonlinear function of this effective stress, but the slow conditions underneath a glacier do not necessarily suggest the use of a sub-aerial correlation. However, Fowler (2010b) found that the streaming instability relied on the existence of a yield stress, something that is essentially also necessary in the sub-aerial case. Our more general results here belie this conclusion.

We non-dimensionalise the equations as previously, with the extra choices

$$b \sim d_D, \quad h_A = 2d_T A, \quad Q \sim q_b, \quad \boldsymbol{\tau}_e \sim \frac{h_0 \tau_b}{2l},$$ (2.36)

where q_b is a typical value of bedload sediment flux. It follows that the dimensionless sediment model is

$$A = \tfrac{1}{2}\left[\frac{\tau}{\mu} - N\right]_+, \quad \tau = f(\bar{u}, N), \quad \boldsymbol{\tau}_e = -h\boldsymbol{\nabla}\psi - \theta\boldsymbol{\nabla}b,$$ (2.37)

and

$$b_t + \boldsymbol{\nabla}.\left[A\bar{u}\mathbf{i}\right] = \beta\boldsymbol{\nabla}.\left[A^3\boldsymbol{\nabla}N\right] - \gamma\boldsymbol{\nabla}.\left[B(\tau_e)\boldsymbol{\tau}_e\right],$$ (2.38)

where we define

$$B(\tau_e) = \frac{Q(\tau_e)}{\tau_e},$$ (2.39)

and the parameters are defined by

$$\beta = \frac{2d_T^2\tau_b}{3\eta_s l_D u_0}, \quad \gamma = \frac{q_b}{d_T u_0}, \quad \theta = \frac{2\Delta\rho_{sw}D_s}{\Delta\rho_{wi}h_0};$$ (2.40)

11

we also define for later use

$$\kappa = \theta\gamma. \tag{2.41}$$

The geometric relation between the ice base and sediment floor is

$$b = s - \delta h, \tag{2.42}$$

where

$$\delta = \frac{h_0}{d_D}. \tag{2.43}$$

2.4 Ice closure

Counting equations, we see that (since $b = s - \delta h$) (2.30) and (2.38) provide two equations for the three unknowns N, s, h, bearing in mind that from (2.30), (2.21), (2.16) and (2.15), $\psi = \psi(N, s, s_t)$. An extra equation is necessary to close the system. In the classical stability theory (Hindmarsh 1998, Fowler 2000), this is taken to be the condition of constant hydraulic potential, $\psi = -N_c$, but in the present context, that is not enough, because we have explicitly introduced the water layer thickness h. Fowler (2009) accommodated $h > 0$ (the formation of cavities) with the extra statement:

$$h = 0 \quad \text{if} \quad N > 0;$$
$$N = 0 \quad \text{if} \quad h > 0, \tag{2.44}$$

and required nothing else.

In the present case, we need an extra equation, because we allow non-zero film thickness even when $N > 0$. This extra condition is the film closure condition, and can be proposed by analogy with the corresponding condition in Röthlisberger's (1972) drainage theory. The necessity for an extra condition occurs because the presence of a partially clast-supported film implies that at the clast separation scale (say metres), a uniform normal (effective) stress in the ice above the bed is partitioned between supporting clasts and the intervening film where it is zero. Thus (Creyts and Schoof 2009) the ice will sink into the film at a rate (for a Glen law model) Kl_cN^n, where K would be proportional to the Glen flow law constant, and l_c is clast spacing. This closure is offset by the production of melt, which thus leads to the closure model

$$h_t = \frac{\rho_w\Gamma}{\rho_i} - Kl_cN^n. \tag{2.45}$$

In this expression, the inter-clast spacing l_c is an increasing function of h, which we may suppose tends to infinity at a critical value h_c, which properly defines a stream (or a cavity), where $h > h_c$. It may be perverse to assume a nonlinear rheology here when ice is considered Newtonian elsewhere, and thus it may be preferable instead to pose the closure condition

$$h_t = \frac{\rho_w\Gamma}{\rho_i} - \frac{l_cN}{\eta_i}. \tag{2.46}$$

Symbol	Meaning	Typical value
a	accumulation rate	0.5 m y^{-1}
b	exponent in sliding law	0.3
d_i	ice depth	10^3 m
D_s	grain size	80 μm
g	gravity	9.8 m s^{-2}
G	geothermal heat flux	0.06 W m^{-2}
k	ice thermal conductivity	2.1 W m^{-1} K^{-1}
l_i	ice sheet length scale	10^3 km
L	latent heat of ice	3.3×10^5 J kg^{-1}
q_b	bedload transport	$\lesssim 0.3$ m^2 y^{-1}
q_T	heat flux to ice	0.06 W m^{-2}
S	ice surface slope	10^{-3}
u_0	ice velocity	100 m y^{-1}
$\Delta\rho_{sw}$	$\rho_s - \rho_w$	1.6×10^3 kg m^{-3}
$\Delta\rho_{wi}$	$\rho_w - \rho_i$	83 kg m^{-3}
ΔT	surface to base temperature change	20 K
η_i	ice viscosity	10^{14} Pa s
η_w	water viscosity	1.8×10^{-3} Pa s
η_s	notional sediment viscosity	2.7×10^9 Pa s
μ	coefficient of friction	0.6
ρ_i	ice density	0.9×10^3 kg m^{-3}
ρ_w	water density	10^3 kg m^{-3}
ρ_s	sediment density	2.6×10^3 kg m^{-3}
ϕ	sediment porosity	0.4

Table 1: Assumed constants in the model.

We will use this expression in what follows.

To non-dimensionalise this, we define a typical clast spacing when $h \sim h_0$ to be l_c^*, and then we write

$$l_c = \frac{l_c^*}{N^*(h)}, \tag{2.47}$$

where h is dimensionless and $N^* \sim O(1)$, so that (2.46) becomes in dimensionless terms

$$\varepsilon r h_t = 1 - \frac{\Pi N}{N^*(h)}, \tag{2.48}$$

where

$$r = \frac{\rho_i}{\rho_w}, \quad \Pi = \frac{\rho_i l_c^* \tau_b}{\rho_w \eta_i \Gamma}. \tag{2.49}$$

The choice of the function $N^*(h)$ is largely one of convenience. We should have $N^* \approx 0$ for $h \gg 1$, $N^* \sim O(1)$ for $h \sim 1$, and $N^* \gtrsim O(1)$ for $h = 0$. In fact, it is best to have $N \to \infty$ as $h \to 0$, since in reality the small neglected melting term in $(2.30)_2$

Symbol	Meaning	Typical value
d_D	drumlin depth	11 m
d_T	till deformation depth	1 m
h_0	water film thickness	6 mm
l_D	drumlin length	640 m
l_c^*	clast spacing	1.2 m
q_w	water flux	3×10^3 m^2 y^{-1}
r	density ratio	0.9
t_D	time scale	74 y
Γ	melt rate	3 mm y^{-1}
τ_b	basal shear stress	0.9×10^4 Pa

Table 2: Derived values of scales.

precludes the film completely disappearing as long as $\omega > 0$. A simple choice which satisfies these constraints is

$$N^* = \frac{1}{h},\tag{2.50}$$

and we use this henceforth. The closure equation thus takes the form

$$\varepsilon r h_t = 1 - \Pi h N.\tag{2.51}$$

2.5   Parameter estimation

The values of the constants which are assumed in the model are given in table 1. Some of these are typical values, and some are intelligent guesses, so that the constant values of the scales in table 2 and table 3 are also representative.

The value of the bedload transport q_b is estimated as follows. Values of q_b/q_w for a turbulent Alpine proglacial stream are of order 10^{-4} (Collins, 1979). We might suppose a similar or lower fraction for the (mostly) slower flow under an ice sheet. The assumption $q_b/q_w \lesssim 10^{-4}$ then leads to $q_b \lesssim 0.3$ m^2 y^{-1}, hence the estimate in table 1.

The simplest way to estimate D_s is to determine it by the critical Shields stress for sediment transport (Fowler 2011, p. 273). The Shields stress is given by

$$\tau^* = \frac{\tau_w}{\Delta \rho_{sw} g D_s},\tag{2.52}$$

where

$$\tau_w = \tfrac{1}{2} h |\boldsymbol{\nabla}\psi| \sim \frac{h_0 \tau_b}{2l}\tag{2.53}$$

is the water film stress. Sediment transport occurs for $\tau^* > \tau_c^*$, where τ_c^* has a typical value of 0.06, but it depends on the particle Reynolds number

$$Re_p = \frac{\rho_w u_* D_s}{\eta_w},\tag{2.54}$$

Symbol	Typical value
α	0.09
β	1.04×10^{-3}
γ	0.3×10^{-2}
δ	0.54×10^{-3}
ε	2.7×10^{-2}
θ	0.62
κ	1.9×10^{-3}
λ	0.78×10^{-2}
ν	1.7×10^{-2}
Π	$\sim O(1)?$
σ	0.64
ω	0.41×10^{-6}

Table 3: Approximate dimensionless parameter values.

where the friction velocity is

$$u_* = \left(\frac{\tau_w}{\rho_w} \right)^{1/2}. \tag{2.55}$$

If we first calculate D_s based on $\tau^* = \tau_c^* \approx 0.06$, we find $D_s \approx 43$ μm, but then $Re_p \sim 0.14$, and at such low values, $\tau_c^* \approx 0.1/Re_p$, which indicates sediment transport if $\tau_w \gtrsim 0.2$ Pa; however, our estimate for τ_w is just 0.04 Pa.

The simple conclusion is that sediment transport need not occur in the millimetric water film, but rather in the cavities which are formed behind growing ribbed moraine. This is essentially the picture portrayed by Fowler (2009) and Chapwanya et $al.$ (2011), and is consistent with an absence of streams. In this case a suitable value of γ is zero, and the specification of D_s is irrelevant. On the other hand, we know that streams do occur, and indeed that floods occur between subglacial lakes (e. g., Engelhardt and Kamb 2013, Sergienko and Hulbe 2011), so some mechanism to form streams must exist. This can be due either to the Walder (1982) thermal mechanism, or due to the pre-emptive formation of cavities and their evolution to a linked cavity system. However, there is also another mechanism which does not rely on fluvial transport. A local thickening of the water film causes a reduction of N, and thus (in a developed rib system, Fowler (2009)) an increase in till deformation depth and thus till flux. This also appears to be a destabilising mechanism. Fowler's (2010b) stream formation mechanism relied on bedload transport, but in that paper the sliding law dependence was explicitly excluded. In either event, we will choose a value of grain size commensurate with transport by a developed stream of depth $h_s = 20$ cm. This gives a water stress of ~ 1.3 Pa, and the Shields criterion suggests $D_s = 80$ μm.

The choice of cooling rate q_T is based on a conductive heat flux $k \Delta T / d_i$, enhanced by horizontal advection; the value in table 1 is enhanced by 1.5. The viscosity η_i would have a normal value of 2×10^{13} Pa s at a shear stress of 10^5 Pa, but two orders of magnitude higher at the lower stress of 10^4 Pa; however this is offset by the

enhancement of shear stress induced by flow over the induced bedforms, so we choose an intermediate value. The 'viscosity' η_s of till is an effective viscosity, if we suppose a normal flow rule. Our estimate is based on the definition

$$\tau_b = \frac{\eta_s u_0}{d_T}, \tag{2.56}$$

which leads to the value in table 1, unsurprisingly consistent with other estimates of this effective value (Paterson 1994, p. 170). It follows from (2.40) that

$$\beta = \frac{2d_T}{3l_D}, \tag{2.57}$$

whence the value in table 3.

The values in table 2 are computed from expressions given in the text. The choice of typical clast spacing l_c^* in table 2 is an essentially arbitrary choice, chosen so that $\Pi \approx 1$. In reality, it should depend on the granulometry of the till, being small for fine grained sediments, and larger for coarser till. However, it should also depend on the small scale roughness of the bed, since if streams form, it would seem that l_c^* should be comparable to stream width.

2.6   A reduced model

The model consists of the equations (2.15), (2.18), (2.16), (2.21), (2.30), (2.37), (2.38), (2.42) and (2.48), which determine b, h, s, ψ, N together with the subsidiary variables A, Φ, Ξ, w, F, $\bar{u}$ and H. For simplicity, we define

$$\psi = -\sigma x + \Psi. \tag{2.58}$$

If we simply proceed with a simplification based on the smallness of the parameters λ and ω, we obtain a reduced model in the form

$$
\begin{aligned}
\sigma(h^3)_x &= \boldsymbol{\nabla}.[h^3 \boldsymbol{\nabla}\psi], \\
\Psi &= s - N + \Phi, \\
A &= \tfrac{1}{2}\left[\frac{f(\bar{u}, N)}{\mu} - N\right]_+, \\
\varepsilon r h_t &= 1 - \Pi h N, \\
b &= s - \delta h, \\
b_t + \boldsymbol{\nabla}.[A\bar{u}\mathbf{i}] + \sigma\gamma[B(\tau_e)h]_x &= \beta\boldsymbol{\nabla}.[A^3\boldsymbol{\nabla}N] + \gamma\boldsymbol{\nabla}.[B(\tau_e)\{h\boldsymbol{\nabla}\Psi + \theta\boldsymbol{\nabla}b\}], \\
\boldsymbol{\tau}_e &= \sigma h\mathbf{i} - \{h\boldsymbol{\nabla}\Psi + \theta\boldsymbol{\nabla}b\}, \\
\alpha s_t + \bar{u}s_x &= w(\Phi, N).
\end{aligned}
\tag{2.59}
$$

We have kept the small terms in β and γ to facilitate the discussion below.

This reduced model can be sensibly compared with that of Fowler (2009). It is in fact the same if $\sigma = 0$ (the apparently inconsequential limit of deep ice) whence

we can take $\psi = -1$ as constant, and neglect β, γ and δ. Consulting (2.59), it seems this is a perfectly good solution. It allows water to trample roughshod over hills, the Creyts–Schoof water film allowing easy passageway.

It can also be compared to Fowler's (2010b) analysis of stream and MSGL formation, which takes $\delta = A = 0$, and replaces (2.51) with the assumption $N = 0$, which would follow from the assumption that $\Pi \gg 1$. It is reasonable to anticipate that the model without both sets of simplifications will admit both forms of the instability.

3   Linear stability

The steady uniform solution of (2.59) is given by

$$ h = 1, \quad N = \frac{1}{\Pi}, \quad b = 0, \quad s = \delta, \quad \Phi = 0, \quad \Psi = \delta - \frac{1}{\Pi}, \quad A = \tfrac{1}{2}\left[\frac{1}{\mu} - \frac{1}{\Pi}\right]. \quad (3.1) $$

Note that this state is actually neutrally stable, since the base levels of h and b are not fixed by the reduced equations. In practice, therefore, it is best to fix the uniform state by means of two specific upstream boundary conditions, for example for two of h, Ψ and b.

Linear stability analysis proceeds along the same lines as in Fowler (2009, 2010b). We write

$$ h = 1 + \bar{h}, \quad N = \frac{1}{\Pi} + \bar{N}, \quad s = \delta + \bar{s}, \quad \Psi = \delta - \frac{1}{\Pi} + \bar{\Psi}; \quad (3.2) $$

linearisation then yields the equations, after some algebra,

$$
\begin{aligned}
3\sigma \bar{h}_x &= \nabla^2 \bar{\Psi}, \\
\bar{\Psi} &= \bar{s} - \bar{N} + \Phi, \\
\varepsilon r \bar{h}_t &= -\bar{h} - \Pi \bar{N}, \\
\bar{s}_t - \delta \bar{h}_t + \bar{u} A' \bar{N}_x &= \beta A^3 \nabla^2 \bar{N} + \gamma \left[B\bar{\Psi}_{yy} + C(\bar{\Psi}_{xx} - \sigma \bar{h}_x)\right], \\
&\quad + \kappa \left[B(\bar{s}_{yy} - \delta \bar{h}_{yy}) + C(\bar{s}_{xx} - \delta \bar{h}_{xx})\right], \\
\alpha \bar{s}_t + \bar{u} \bar{s}_x &= J * \Phi + f_N L * \bar{N}, \quad (3.3)
\end{aligned}
$$

where A, $A' = A'(N)$ and $f_N = \partial f / \partial N$ are evaluated at the basic state (3.1), κ was defined in (2.41), and

$$ C = B + \sigma B'. \quad (3.4) $$

For the sliding law in (2.19), we have

$$ f_N = b\Pi. \quad (3.5) $$

Note that, using (2.39),

$$ C = Q', \quad (3.6) $$

17

where Q is the dimensionless bedload flux, evaluated at the base state $\tau_e = \sigma$. Defining the Fourier transform $\hat{f}$ of $\bar{f}$ as in (2.20) and taking $\hat{f} = \tilde{f}e^{\Sigma t}$, we find

$$
\begin{aligned}
3\sigma i k_1 \tilde{h} &= k^2 \tilde{\Psi}, \\
\tilde{\Psi} &= [M + 2kU\alpha\Sigma]\tilde{s} - (1 + f_N V)\tilde{N}, \\
\varepsilon r \Sigma \tilde{h} &= -\tilde{h} - \Pi\tilde{N}, \\
(\Sigma + T)(\tilde{s} - \delta\tilde{h}) - S\tilde{N} &= E\tilde{\Psi},
\end{aligned}
\tag{3.7}
$$

where we define

$$
\begin{aligned}
E &= \gamma[(\tfrac{1}{3}C - B)k_2^2 - \tfrac{2}{3}Ck_1^2], \\
T &= \kappa(Bk_2^2 + Ck_1^2), \\
M &= 1 - 2ik_1 k\bar{u}U, \\
S &= ik_1 \bar{u}A' - \beta A^3 k^2, \\
U = \frac{1}{2k\hat{J}} &= \frac{j + S_h C_h}{S_h^2}, \\
V = \frac{\hat{L}}{\hat{J}} &= \frac{ik_1 j}{kS_h^2}
\end{aligned}
\tag{3.8}
$$

(cf. (2.25)). The zero determinant condition for a solution of these yields a quadratic equation for the growth rate Σ:

$$
f_2 \Sigma^2 + f_1 \Sigma + f_0 = 0,
\tag{3.9}
$$

where

$$
\begin{aligned}
f_2 &= [\varepsilon r P + 2\delta\alpha\Pi kU]k^2, \\
f_1 &= -3\sigma i k_1 \Pi W + k^2[P - \varepsilon r\{SM - (1 + f_N V)T\} + \delta\Pi(M + 2\alpha kUT)], \\
f_0 &= M(3\sigma i k_1 \Pi E - k^2 S) + T\{(1 + f_N V + \delta\Pi M)k^2 - 3\sigma i k_1 \Pi\},
\end{aligned}
\tag{3.10}
$$

and also

$$
\begin{aligned}
W &= 1 - 2\alpha kUE, \\
P &= 1 + f_N V - 2\alpha kUS.
\end{aligned}
\tag{3.11}
$$

The two roots are given by

$$
\Sigma_\pm = \frac{\pm(f_1^2 - 4f_0 f_2)^{1/2} - f_1}{2f_2},
\tag{3.12}
$$

and we shall primarily be interested in Σ_+.

Simplification of (3.9) follows from neglecting the small coefficients β, κ (thus also T) and δ; then the quadratic takes the simpler form

$$\varepsilon r P k^2 \Sigma^2 - [3\sigma i k_1 \Pi W - k^2 (P - \varepsilon r S M)]\Sigma + M(3\sigma i k_1 \Pi E - k^2 S) = 0. \qquad (3.13)$$

Because also $\varepsilon \ll 1$, there is a fast root (which is Σ_-) of $O\left(\dfrac{1}{\varepsilon}\right)$, which is easily found to be stable (it represents the rapid relaxation of the film closure equation to equilibrium), and a slow root, which for $\varepsilon \to 0$, is given by

$$\Sigma = \frac{M(3\sigma i k_1 \Pi E - k^2 S)}{3\sigma i k_1 \Pi W - k^2 P}. \qquad (3.14)$$

This expression generalises the stability analyses of Fowler (2009) and Fowler (2010b). In particular, the ribbing instability result (2.16) of Fowler (2009),

$$\Sigma = \frac{MS}{P} = \frac{i k_1 \bar{u} A'(1 - 2i k_1 k\bar{u})}{1 - 2i k_1 k\alpha \bar{u} A'}, \qquad (3.15)$$

is regained in the limits $\sigma\Pi = 0$ and $j \to \infty$ (deep ice, thus $U = 1$ and $V = 0$), under the identification

$$R = \bar{u} A', \qquad (3.16)$$

while the MSGL result (3.11) of Fowler (2010b) is regained in the limits $\sigma\Pi \to \infty$ and $j \to \infty$:

$$\Sigma = \frac{ME}{W} = \frac{(1 - 2i k_1 k\bar{u})E}{1 - 2\alpha k E}. \qquad (3.17)$$

(The coefficient D in the 2010 paper is absent as it arises from the neglected terms in T in (3.10).)

A question of some interest is how the maximal growth rate depends on k_1 and k_2. Remember, this was one of the issues concerning the instability theory: there seemed to be no genuine three-dimensional instabilities. Figure 4 shows contour maps of growth rate in conditions of instability, when $R = \bar{u} A' > 0$. Ribs, drumlins or MSGL are the preferred mode depending on the value of Π. Specifically, transverse ridges (ribbed moraine) are preferred for small values of Π, while longitudinal ridges (lineations) are preferred for large Π; and for intermediate values, the maximal growth rate occurs for genuinely three-dimensional drumlinoid shapes.

A comment on these results is necessary. Firstly, while the approximate result (3.14) is indeed valid as $\varepsilon \to 0$, it is actually not accurate for our estimated value $\varepsilon = 2.7 \times 10^{-2}$, apparently because the maximal growth rates occur for $k \gtrsim 3$ (so εk^2 is not small). With the selected parameter values, accuracy ensues for $\varepsilon \lesssim 0.5 \times 10^{-3}$, although lower values of Π make the approximate result more robust. One noteworthy comment is that the MSGL instability criterion of Fowler (2010b) required $C > 3B$ in order that $E > 0$. In the present combined theory, this criterion is not necessary. Indeed, approximation of the values of Σ_+ taking $\beta = \gamma = \delta = \kappa = 0$ has minimal effect on the results.
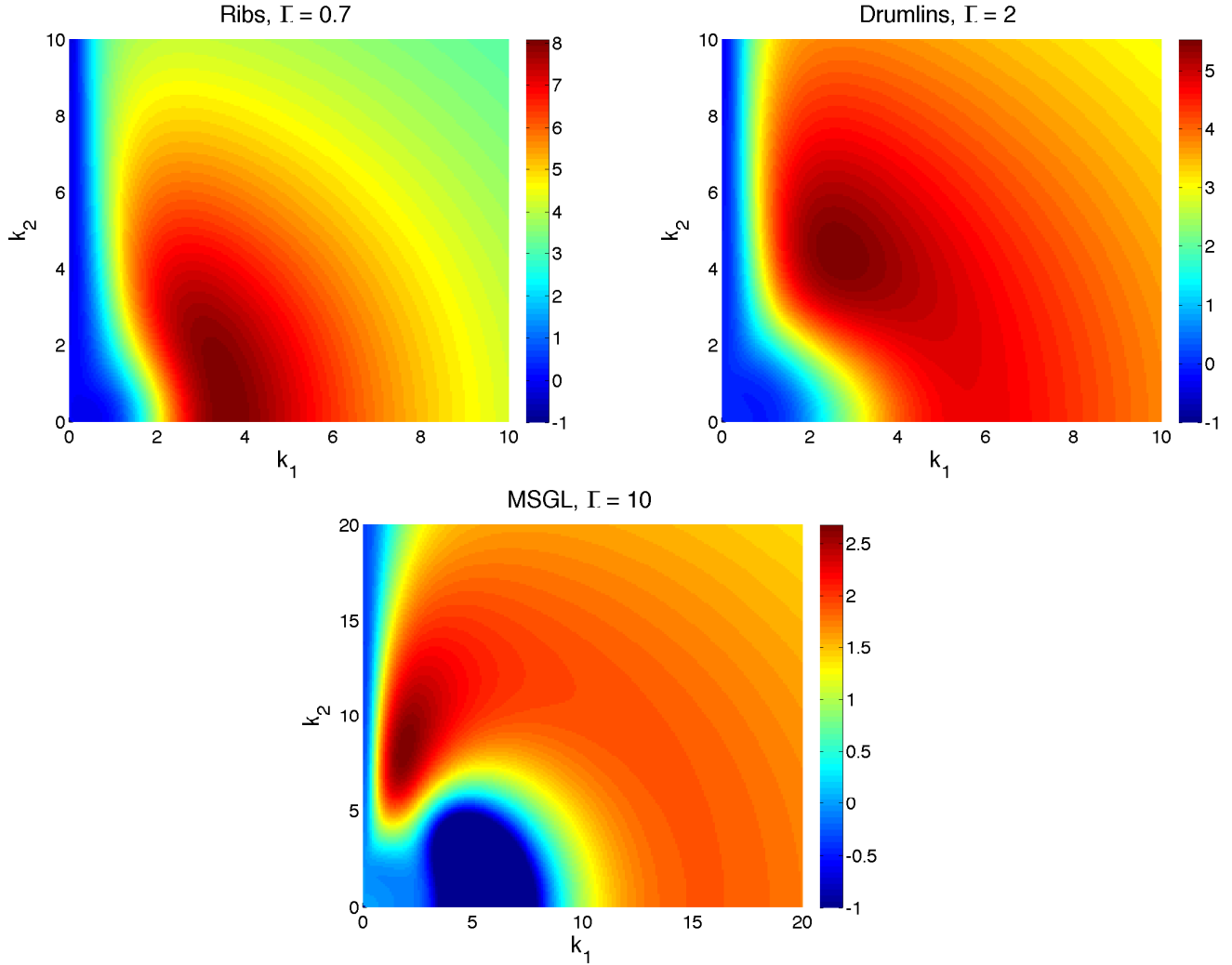
Figure 4: Contour plots of $\operatorname{Re}\Sigma_+$ as defined in (3.12), for parameter values $\alpha = 0.1$, $\beta = 10^{-3}$, $\gamma = 0.3 \times 10^{-2}$, $\delta = 0.5 \times 10^{-3}$, $\varepsilon = 2.7 \times 10^{-2}$, $\kappa = 2 \times 10^{-3}$, $\mu = 0.6$, $\sigma = 0.64$, $b = 0.3$, $C = 1$, $B = 1$, $\bar{u} = 1$, $R = \bar{u}A' = 1$, and with values $\Pi = 0.7$ (top left), $= 2$ (top right), and $= 10$ (bottom), corresponding to ribs, drumlins and MSGL respectively. The negative growth rates are truncated at $\operatorname{Re}\Sigma_+ = -1$ in order to enhance the colour contrast. Note the different wavenumber scales in the MSGL figure, and the different colour scales in each figure.

Plotting of these results in terms of length and width (defined as half-periods) is of potential use in comparison with observed data, although it must be borne in mind that linear stability results do not necessarily bear close relation to observed finite amplitude results. An example of such a plot is in figure 5, where the regions of maximal growth lie close to observed ranges of actual bedforms (Clark *et al.* 2009, Stokes *et al.* 2013b, Ely 2014), though the mega-ribs of Greenwood and Kleman (2010) and the similarly-sized traction ribs of Sergienko and Hindmarsh (2013) are somewhat
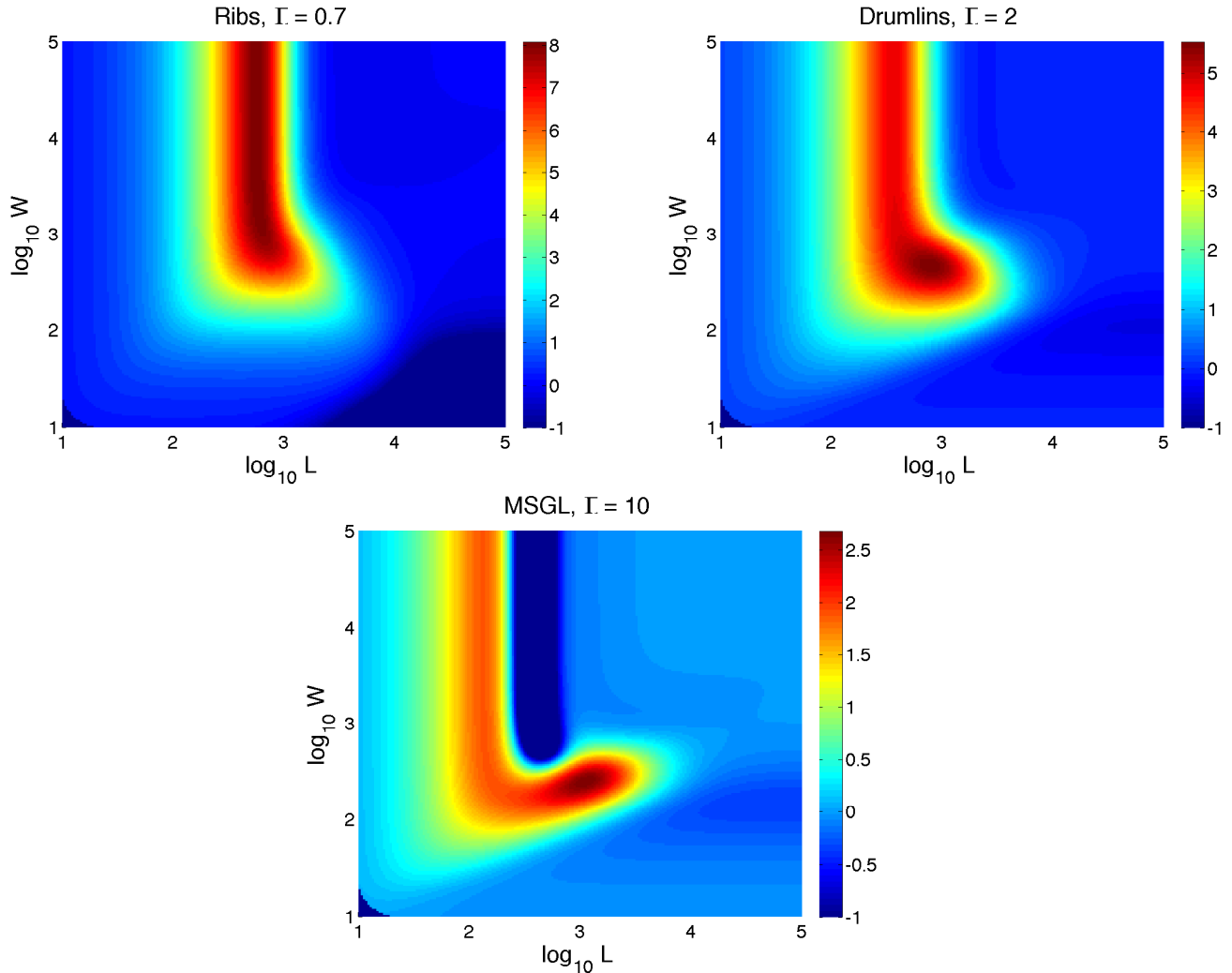
Figure 5: As for figure 4, but plotted in terms of logarithms to the base ten of dimensional length L and width W (in metres), defined in terms of k_1 and k_2 by $L = \dfrac{\pi l_D}{k_1}$, $W = \dfrac{\pi l_D}{k_2}$, $l_D = 640$ m. This enables comparison with similar plots of corresponding observed bedforms (Clark *et al.* 2009, Stokes *et al.* 2013b, Ely 2014). The small blue regions at the bottom left are numerical artefacts, due to Matlab's unwillingness to calculate $\sinh^2 j$ for $j > 355$.

larger. In particular, the suggestion of our theory that ribs, drumlins and lineations all form through a single process appears to be consistent with observed length-width distributions of these various bedforms, which appear to form overlapping clusters in parameter space (Ely 2014).

Of possible interest, or possible concern, is the retention of the ribbing mode as Π increases, although it becomes weaker. By comparison with figure 4, this may be associated with the fact that $\mathrm{Re}\,\Sigma_+$ decreases slowly to zero as k increases, and does not become negative at large wave number. We suspect this may be associated with

21

oversimplified physics, which does not provide a stabilising mechanism at large wave number, and we expect this may be associated with an over-simple closure relation, which lacks any spatial derivatives.

However, we should also point out the danger of trying to over-interpret figure 5. It is merely a linear stability diagram, and can only give hints of finite amplitude observations. Ribbed moraine has a fairly definite preferred width to length ratio of about three to four (Ely 2014). Infinitely wide ribs do not occur, and this may be due to the necessity to provide a passageway for the downstream flow of water .

4 Conclusions

In this paper we have provided a theoretical model for the coupled evolution of ice, water and sediment at the base of an ice sheet. The theory is a development of earlier more rudimentary versions, and the principal theoretical development presented here lies in the consideration of the water in a Creyts–Schoof water film. This concept securely allows a water film at the base without the associated unrealities of flotation and vanishing stress.

The model consists essentially of four partial differential equations, representing evolution of basal ice surface (2.24), conservation of water mass (2.30), conservation of sediment (2.38), and ice closure (2.48). The first three of these are securely based on physical principles, but the provenance of the closure equation is less clear, despite its familiarity in the case of Röthlisberger channels, since it seems that the ice surface kinematic equation (2.24) ought to represent the same physical process. The argument that both equations are necessary is based on scale: the closure equation represents ice motion at the microscale of the water film, while the kinematic equation represents the macroscopic ice motion associated with flow over the bed. The distinction is similar to the scale separation used in determining the sliding law (Fowler 1981).

The earliest versions of the instability theory assumed a passive, hydrostatic water system. In this latest edition of the model, we have included a fully integrated water system in the form of a Creyts–Schoof film, with the included ability to describe both streams and cavities. Analysis of the instability of the uniform state of the system shows that the preferred mode of spatial growth (and thus what might correspond to the actual observed pattern) ranges from ribbed moraine pattern through drumlin pattern to glacial lineation pattern as a single critical dimensionless parameter Π increases from 0.7 to 10. In fact, consultation of (3.10) suggests (since δ is small) that it is the product $\sigma\Pi$ which is important.

The fact that this parameter is a product suggests a complicated combination of stability-determining circumstances. In particular, the fact that σ is the ratio of the drumlin length scale l_D to the ice depth scale d_i suggests that, in contradiction to earlier results (e. g., Fowler 2009), ice depth is an important quantity. Actually, this appears not to be the case, and it is better to view $\sigma\Pi$ as a single controlling parameter. From (2.7), (2.12), (2.49) and (2.10), it is defined by

$$\sigma\Pi = \frac{\rho_i^2}{\rho_w}\left(\frac{g}{\Delta\rho_{wi}}\right)^{1/2}\frac{l_c^*}{\Gamma}\left(\frac{u_0}{\eta_i}\right)^{1/2}, \tag{4.1}$$

where also the basal melting term Γ is defined in (2.28), and we see that it is in fact independent of ice depth. A simple rescaling in (2.10) and (2.11) using l_D instead of d_i would lead to the parameter defined above appearing in the closure equation.

The principal dependence of $\sigma\Pi$ is on the clast spacing l_c^*, and if we had to make a prediction based on this definition, it would be that fine-grained sediments (large l_c^*) would promote lineations, while coarser tills (small l_c^*) promote ribs or drumlins. The dependence on ice velocity is relatively weak; we might take $\Gamma \sim \tau_b u_0$ and $\eta_i \propto \tau_b^{-2}$, in which case $\sigma\Pi \sim u_0^{-1/2}$, but the consequent variation of $\sigma\Pi$ is rather small.

The dependence of the results of this analysis on the clast spacing is intriguing but also frustrating. The closure equation is the least satisfactory part of the model, and a sensible definition of l_c^* necessarily hard to tie down. Earlier we chose $l_c^* = 1.2$ m, ostensibly so that $\Pi \sim 1$. A more intelligent choice would be such that the dimensional equilibrium value $N = \tau_b/\Pi$ corresponds to observed values, commonly thought to be 0.5 bar $= 5 \times 10^4$ Pa beneath Whillans Ice Stream (Blankenship *et al.* 1987). Using the value of τ_b in table 2, this suggests $\Pi = 0.18$, corresponding to a choice $l_c^* = 0.21$ m. Note, however, that we require $\tau_b > \mu N$ is the till is to deform, corresponding to $\Pi > \mu$. The issue is clouded in practice by the observation that much of the resistance in Antarctic ice streams is provided by lateral drag, as opposed to the basal drag as asssumed here (Van der Veen 1999).

This discussion is not very encouraging, because it suggests (see figure 4) that high values of l_c^*, perhaps of order 10 m, are necessary to form MSGL, and this seems unlikely for fine-grained till. Nor, however, is it very conclusive. Indeed, we consider it likely in reality that water flow over fine-grained till will form shallow streams, whose width will then become the measure of effective clast spacing.

So we think that the rôle of the clast spacing, and the provision of the closure equation, will require an increasing sophistication in future development of this theory; in particular, while the present form may be reasonable for ice flow over a macroscopically flat bed, we suspect that a more elaborate version will be necessary in the presence of streams or bed topography. One possible development may involve the prescription of l_c as a non-local function of film thickness h, to allow for the situation where full stream separation occurs. A related point may be the slow decay of growth rate in figure 4. Using the approximation (3.14), the growth rate is

$$\operatorname{Re}\Sigma = \frac{k_1^2(3\sigma\Pi E - k^2 R)(3\sigma\Pi W + 2\alpha k^3 R - 2k^3\bar{u})}{k^4 + k_1^2(3\sigma\Pi W + 2\alpha k^3 R)^2}, \qquad (4.2)$$

which shows that $\operatorname{Re}\Sigma \sim O\left(\dfrac{1}{k}\right)$ as $k \to \infty$. In a well-posed model, one hopes for diffusive decay of growth rate at large wave number, e. g., $\operatorname{Re}\Sigma \sim -k^2$, and it is possible that more sophisticated closure models will allow this. In particular, it is likely that this slow decay is a contributor to our present problems in providing numerical solutions of the model.

Acknowledgements

References

Bindschadler, R. A. 1983 The importance of pressurized subglacial water in separation and sliding at the glacier bed. J. Glaciol. **29** (101), 3–19.

Blankenship, D. D., C. R. Bentley, S. T. Rooney and R. B. Alley 1987 Till beneath Ice Stream B. 1. Properties derived from seismic travel times. J. Geophys. Res. **92** (B9), 8,903–8,911.

Boulton, G. S. 1987 A theory of drumlin formation by subglacial sediment deformation. In: *Drumlin symposium*, eds. J. Menzies and J. Rose, Balkema, Rotterdam, pp. 25–80.

Bryce, J. 1833 On the evidences of diluvial action in the north of Ireland. J. Geol. Soc. Dubl. **1**, 34–44.

Chapwanya, M., C. D. Clark and A. C. Fowler 2011 Numerical computations of a theoretical model of ribbed moraine formation. Earth Surf. Proc. Landf. **36**, 1,105–1,112.

Clark, C. D. 1993 Mega-scale glacial lineations and cross-cutting ice-flow landforms. Earth Surf. Proc. Landf. **18**, 1–29.

Clark, C. D. 2010 Emergent drumlins and their clones: from till dilatancy to flow instabilities. J. Glaciol. **51**, 1,011–1,025.

Clark, C. D., A. L. C. Hughes, S. L. Greenwood, M. Spagnolo, and F. S.Ł. Ng, 2009 Size and shape characteristics of drumlins, derived from a large sample, and associated scaling laws. Quat. Sci. Revs. **28**, 677–692.

Collins, D. N. 1979 Sediment concentration in melt waters as an indicator of erosion processes beneath an Alpine glacier. J. Glaciol. **23**, 247–257.

Creyts, T. T. and C. G. Schoof 2009 Drainage through subglacial water sheets. J. Geophys. Res. **114**, F04008, doi:10.1029/2008JF001215.

Dunlop, P. and C. D. Clark 2006 The morphological characteristics of ribbed moraine. Quat. Sci. Revs. **25**, 1,668–1,691.

Dunlop, P., C. D. Clark, and R. C. A. Hindmarsh 2008 Bed ribbing instability explanation: testing a numerical model of ribbed moraine formation arising from coupled flow of ice and subglacial sediment. J. Geophys. Res. **113**, F03005, doi:10.1029/2007JF000954.

Ely, J. C. 2014 Flow signatures on the bed and the surface of ice sheets: insights into their characteristics and formation. Ph. D. thesis, University of Sheffield.

Engelhardt, H. and B. Kamb 2013 Kamb Ice Stream flow history and surge potential. Ann. Glaciol. **54**, 287–298.

Fisher, T. G. and J. Shaw 1992 A depositional model for Rogen moraine, with examples from the Avalon Peninsula, Newfoundland. Can. J. Earth Sci. **29**, 669–686.

Fowler, A. C. 1981 A theoretical treatment of the sliding of glaciers in the absence of cavitation. Phil. Trans. R. Soc. Lond. A**298**, 637–685.

Fowler, A. C. 2000 An instability mechanism for drumlin formation. In: *Deformation of subglacial materials*, eds. A. Maltman, M. J. Hambrey and B. Hubbard, Spec. Pub. Geol. Soc. **176**, pp. 307–319. The Geological Society, London.

Fowler, A. C. 2009 Instability modelling of drumlin formation incorporating lee-side cavity growth. Proc. R. Soc. Lond. A**465**, 2681–2702, doi:10.1098/rspa.2008.0490.

Fowler, A. C. 2010a The instability theory of drumlin formation applied to Newtonian viscous ice of finite depth. Proc. R. Soc. Lond. A**466**, 2,673–2,694. doi: 10.1098/rspa.2010.0017.

Fowler, A. C. 2010b The formation of subglacial streams and mega-scale glacial lineations. Proc. R. Soc. Lond. A**466**, 3,181–3,201. doi: 10.1098/rspa.2010.0009.

Fowler, A. C. 2011 Mathematical geoscience. Springer-Verlag, London.

Gravenor, C. P. 1953 The origin of drumins. Amer. J. Sci. **251**, 674–681.

Greenwood, S. L. and J. Kleman 2010 Glacial landforms of extreme size in the Keewatin sector of the Laurentide Ice Sheet. Quat. Sci. Revs. **29**, 1,894–1,910.

Hart, J. K. 2005 Thornhill drumlin. In: Coxon, P. (ed.), The Quaternary of West Central Ireland, Field Guide. Quaternary Research Association, London, pp. 193–201.

Hättestrand, C. and J. Kleman 1999 Ribbed moraine formation. Quat. Sci. Revs. **18**, 43–61.

Henann, D. L. and K. Kamrin 2013 A predictive, size-dependent continuum model for dense granular flows. PNAS **110**, 6,730–6735.

Hiemstra, J. F., B. Kulessa, E. C. King and D. Ntarlagiannis 2011 The use of integrated sedimentological and geophysical methods in drumlin research—a case study of Pigeon Point, Clew Bay, Northwest Ireland. Earth Surf. Process. Landf. **26**, 1,860–1,871.

Hindmarsh, R. C. A. 1998 The stability of a viscous till sheet coupled with ice flow, considered at wavelengths less than the ice thickness. J. Glaciol. **44** (146), 285–292.

Kinahan, G. H. and M. H. Close 1872 The general glaciation of Iar-Connaught and its neighbourhood, in the counties of Galway and Mayo. Hodges, Foster and Co., Dublin.

Kleman, J. and C. Hättestrand 1999 Frozen-bed Fennoscandian and Laurentide ice sheets during the last glacial maximum. Nature **402**, 63–66.

Kyrke-Smith, T. M., R. F. Katz and A. C. Fowler 2014 Subglacial hydrology and the formation of ice streams. Proc. R. Soc. Lond. A**470**, 20130494.

Lindén, M., P. Möller and L. Adrielson 2008 Ribbed moraine formed by subglacial folding, thrust stacking and lee-side cavity infill. Boreas **37**, 102–131.

Lundqvist, J. 1969 Problems of the so-called Rogen moraine. Sveriges Geologiska Undersökning C 648. 32 pp.

Menzies, J. M. 1979a The mechanics of drumlin formation with particular reference to the change in pore-water content of the till. J. Glaciol. **22**, 373–384.

Menzies, J. 1979b A review of the literature on the formation and location of drumlins. Earth Sci. Rev. **14**, 315–359.

Möller, P. 2006 Rogen moraine: an example of glacial re-shaping of pre-existing landforms. Quat. Sci. Revs., **25**, 362–389.

Möller, P. 2010 Melt-out till and ribbed moraine formation, a case study from south Sweden. Sed. Geol., in press. doi: 10.1016/j.sedgeo.2009.11.003.

Paterson, W. S. B. 1994 The physics of glaciers, 3rd ed. Butterworth–Heinemann, Oxford.

Pelletier, J. D. 2008 Quantitative modeling of Earth surface processes. C. U. P., Cambridge.

Röthlisberger, H. 1972 Water pressure in intra- and subglacial channels. J. Glaciol. **11**, 177–203.

Schoof, C. 2007a Pressure-dependent viscosity and interfacial instability in coupled ice-sediment flow. J. Fluid Mech. **570**, 227–252.

Schoof, C. 2007b Cavitation in deformable glacier beds. SIAM J. Appl. Math. **67**, 1,633–1,653.

Schoof, C. and G. K. C. Clarke 2008 A model of spiral flows in basal ice and the formation of subglacial flutes based on a Reiner–Rivlin rheology for glacial ice. J. Geophys. Res. **13**, B05204.

Sergienko, O. V. and R. C. A. Hindmarsh 2013 Regular patterns in frictional resistance of ice-stream beds seen by surface data inversion. Science **342** (6162), 1,086–1,089.

Sergienko, O. V. and C. L. Hulbe 2011 'Sticky spots' and subglacial lakes under ice streams of the Siple Coast, Antarctica. Ann. Glaciol. **52**, 18–22.

Smalley, I. J. and D. J. Unwin 1968 The formation and shape of drumlins and their distribution and orientation in drumlin fields. J. Glaciol. **7**, 377–390.

Smith, T. R. and F. P. Bretherton 1972 Stability and the conservation of mass in drainage basin evolution. Water Resour. Res. **8**, 1506–1529.

Stokes, C. R., A. C. Fowler, C. D. Clark, R. C. A. Hindmarsh and M. Spagnolo 2013a The instability theory of drumlin formation and its explanation of their varied composition and internal structure. Quat. Sci. Revs. **62**, 77–96.

Stokes, C. R., M. Spagnolo, C. D. Clark, C. Ó Cofaigh, O. B. Lian and R. B. Dunstone 2013b Formation of mega-scale glacial lineations on the Dubawnt Lake Ice Stream bed: 1. size, shape and spacing from a large remote sensing dataset. Quat. Sci. Revs. **77**, 190–209.

Sugden, D. E. and B. S. John 1976 Glaciers and landscape. Edward Arnold, London.

Van der Veen, C. J. 1999 Fundamentals of glacier dynamics. A. A. Balkema, Rotterdam.

Walder, J. S. 1982 Stability of sheet flow of water beneath temperate glaciers and implications for glacier surging. J. Glaciol. **28**, 273–293.